Large-Signal Spurious-Free Dynamic Range Due to Static and Dynamic Clipping in Direct and External Modulation Systems

Benjamin H. Wang, *Member, IEEE,* Pi-Yang Chiang, *Member, IEEE,* Ming-Seng Kao, *Member, IEEE,* and Winston I. Way, *Senior Member, IEEE, Fellow, OSA*

***Abstract*— Large-signal spurious-free dynamic range (SFDR) is useful in an optical system with a high intensity noise level, which can be due to optical reflections or optical beat interference, and with large modulating signals to achieve sufficient carrier-to-noise ratio (CNR). A closed-form analysis on large-signal SFDR due to static and dynamic clipping for direct and external modulation systems is presented in this paper. The analysis can be applied to laser diodes (LD's) and external modulators with arbitrary transfer functions. We have used the analysis to predict the theoretical upper-bound for large-signal SFDR due to static clipping in an ideal LD and external modulators with various linearization techniques. We have also used the analysis to predict the dynamic-clipping-induced nonlinear distortions (NLD's) in a weakly clipped LD, and confirm that dynamic clipping is more important to consider than static clipping when weak LD clipping takes place. Large-signal SFDR's in practical LD's and external modulators were also compared. The validity of our analysis is confirmed through computer simulation and actual measurement of clipping-induced NLD's in a typical CATV-quality DFB LD.**

***Index Terms*—Dynamic clipping, purious-free dynamic range, subcarrier multiplexed system.**

I. Introduction

TWO-TONE spurious-free dynamic range (SFDR) is defined as the carrier-to-noise ratio (CNR) when the noise floor in the signal bandwidth equals to the third-order intermodulation (IM_3) products [1]–[4]. It has been widely used to simultaneously characterize the linearity and noise characteristics of microwave devices (e.g., amplifiers, mixers, etc.), analog-to-digital converters [5]–[6], and optical devices such as laser diodes (LD's) and external modulators [1]–[4]. Two-tone SFDR is conventionally defined with respect to small input signals, and narrow-band signals such as wireless, digital microwave, and satellite signals. Owing to the small-signal and narrow-band assumptions in defining SFDR, therefore, one only has to consider IM_3 products.

Recently, however, the feasibility of clipping-limited large-signal modulation in both direct [7] and external modulation [8]–[9] subcarrier multiplexed (SCM) systems have been investigated, mainly for the purpose of increasing transmission distance and link budget through increasing optical modulation index (OMI) per carrier. But these studies have been mostly concentrated on the case of multiple equal-amplitude channels, which has an aggregated Gaussian statistics [10]–[13]. Since SFDR is defined and measured based on two tones whose aggregated statistics is significantly different from Gaussian [14], there is a need to find a new analytical approach to obtain a closed-form result of clipping-limited, large-signal SFDR. We will show that a large-signal SFDR is (linearly or nonlinearly) inversely proportional to OMI/carrier. This is quite different from the case of a small-signal SFDR which is OMI-independent [2]. Therefore, when considering large-signal SFDR, there is a tradeoff between SFDR and system power budget. This is because the latter is (linearly or nonlinearly) proportional to OMI.

Large-signal SFDR is also needed from the standpoint that the noise floor in a signal bandwidth can be very large in some system applications. For example, relative intensity noise (RIN) due to optical reflections [15] or optical beat interference [16]–[19] can be as high as -95 to -120 dB/Hz. In this case, a large-signal modulation may be needed to overcome the high noise floor in order to maintain a required CNR, and consequently clipping-induced IM products may occur [20].

Conventionally, the analysis of clipping-induced NLD's has always been based on the assumption of static clipping [11]–[13], i.e., the clipping phenomenon is not frequency-dependent, which is generally true for external modulators. The analytical result thus obtained can be used as an upper bound on the channel capacity of an optical transmitter. However, it has been recently found that this upper bound is over-optimistic for a LD, because nonlinear distortions (NLD's) due to dynamic clipping cannot be ignored [20]–[24]. The NLD's due to dynamic clipping are different from those caused by laser relaxation oscillation frequency, and can cause a significant turn-on delay in a modulating sinusoidal signal. In particular, dynamic clipping can dominate over other nonlinear mechanisms when a LD is weakly clipped. Therefore, the effect of dynamic clipping on SFDR must be carefully examined.

In this paper, we investigate the SFDR due to static and dynamic clipping in direct and external modulation systems. Closed-form solutions of carrier-to-intermodulation ratio (C/IM) based on spectral analysis [7], [12], [25] are provided in Section II for optical transmitters with arbitrary transfer functions. The concept and analysis of large-signal SFDR are provided in Section II. Computer simulation results are

Manuscript received February 18, 1998; revised June 26, 1998.

The authors are with the Department of Communication Engineering, National Chiao-Tung University, Hsinchu, Taiwan, China.

Publisher Item Identifier S 0733-8724(98)07402-7.

given in Section III to verify the closed-form derivations. To investigate the effect of LD dynamic clipping, we also carried out several experiments in this paper. The measurement of an L-I curve when a LD is under dynamic clipping is described in Section IV. Based on the measured dynamically clipped L-I curve, the IM products of a clipped-LD are calculated by using the closed-form formulae derived in Section II. The calculated results are compared with the measured ones in Section V. The clipping-limited SFDR performances for LD's and external modulators are provided in Section VI. Further discussion on the concept of large-signal SFDR's is included in Section VII. Our conclusion is given in Section VIII.

II. Analysis

A. Closed-Form Solution for Two-Tone IM Products

We start with the two-tone modulating signal $I(t)$ given by

$$I(t) = I_b + I_m[\cos(\omega_1 t + \phi_1) + \cos(\omega_2 t + \phi_2)] \quad (1)$$

where I_b is the bias current, I_m is the amplitude of each modulating carrier, and ϕ_1, ϕ_2 are two independent random phases uniformly distributed in [0, 2π]. The amplitude I_m equals to m $(I_b - I_{th}$ where I_{th} is the laser threshold and m is the electrical modulation index per carrier and is assumed to be equivalent to OMI/carrier. Assuming the transfer function of a LD is given by $g(\cdot)$, i.e. $g(\cdot)$ represents the L-I (light power versus bias current) curve, the optical intensity $y(t)$ can be written as $y(t) = g(I(t))$ (in case of external modulators, the modulating current $I(t)$ should be replaced by the modulating voltage $V(t)$ and $g(\cdot)$ represents the L-V curve). The autocorrelation function $R_y(\tau)$ of $y(t)$ is given as [25]

$$\begin{aligned} R_y(\tau) &= E\{y(t+\tau)y(t)\} \\ &= \int_{-\infty}^{infty}\int_{-\infty}^{\infty} G(f_1)G(f_2) \\ &\quad \cdot E\{\exp(j2\pi f_1 I(t+\tau))\exp(j2\pi f_2 I(t))\}\, df_1\, df_2 \end{aligned} \quad (2)$$

where $E\{\cdot\}$ is the expectation operator and $G(\cdot)$ is the Fourier transform of $g(\cdot)$. Substituting (1) into (2), we can obtain $R_y(\tau)$ as

$$\begin{aligned} R_y(\tau) = \int_{-\infty}^{\infty}\int_{-\infty}^{\infty} & G(f_1)G(f_2)\exp(j2\pi f_1 I_b) \\ & \cdot \exp(j2\pi f_2 I_b) J_0(\beta_1) J_0(\beta_2)\, df_1\, df_2 \end{aligned} \quad (3)$$

where $J_o(\cdot)$ is the zeroth-order Bessel function of the first kind, and

$$\begin{aligned} \beta_1 &= \sqrt{r_1^2 + r_2^2 + 2r_1 r_2 \cos(\omega_1 \tau)} \\ \beta_2 &= \sqrt{r_1^2 + r_2^2 + 2r_1 r_2 \cos(\omega_2 \tau)} \end{aligned} \quad (4)$$

and

$$\begin{aligned} r_1 &= 2\pi f_1 I_m \\ r_2 &= 2\pi f_2 I_m. \end{aligned} \quad (5)$$

Note that $J_o(\beta_1)\ J_o(\beta_2)$ can be expanded as

$$\begin{aligned} &J_o(\beta_1)J_o(\beta_2) \\ &\quad = [J_0(r_1)J_0(r_2)]^2 \\ &\qquad + 2J_0(r_1)J_0(r_2)\left\{\sum_{k=1}^{\infty} J_k(r_1)J_k(r_2)(-1)^k \cos(k\omega_1\tau)\right. \\ &\qquad \left. \cdot \sum_{n=1}^{\infty} J_n(r_1)J_n(r_2)(-1)^n \cos(n\omega_2\tau)\right\} \\ &\qquad + 4\left\{\sum_{k=1}^{\infty} J_k(r_1)J_k(r_2)(-1)^k \cos(k\omega_1\tau)\right\} \\ &\qquad \cdot \left\{\sum_{n=1}^{\infty} J_n(r_1)J_n(r_2)(-1)^n \cos(n\omega_2\tau)\right\} \end{aligned} \quad (6)$$

where $J_k(\cdot)$ is the kth order Bessel function of the first kind. From (3) and (6), the output autocorrelation function of an arbitrary IM product at $k\omega_1 \pm n\omega_2$ can be obtained as

$$\begin{aligned} R_{k\omega_1 \pm n\omega_2}(\tau) &= 2(-1)^{k+n} \\ &\quad \cdot \left[\int_{-\infty}^{\infty} G(f)\exp(j2\pi f I_b) J_k(r) J_n(r)\, df\right]^2 \\ &\quad \cdot \cos((k\omega_1 \pm n\omega_2)\tau) \end{aligned} \quad (7)$$

where $r = 2\pi f I_m$. The output autocorrelation function for fundamental frequency components at ω_1 and ω_2 are obtained by letting $k = 1, n = 0$, and $n = 1, k = 0$, respectively, and for any order of IM product can be obtained with $k \neq 0$ and $n \neq 0$. Consequently, mean square current of any frequency component, $\langle i^2_{k\omega_1 \pm n\omega_2}\rangle$, due to two-tone modulation can be obtained by setting $\tau = 0$ in the autocorrelation function $R_{k\omega_1, \pm n\omega_2}$, and is given by

$$\begin{aligned} \langle i^2_{k\omega_1 \pm n\omega_2}\rangle &= 2(-1)^{k+n} \\ &\quad \cdot \left[\int_{-\infty}^{\infty} G(f)\exp(j2\pi f I_b) J_k(r) J_n(r)\, df\right]^2. \end{aligned} \quad (8)$$

Given a (static or dynamic) laser L-I curve $g(x)$, (8) can be rewritten as

$$\begin{aligned} \langle i^2_{k\omega_1 \pm n\omega_2}\rangle &= 2(-1)^{k+n} \\ &\quad \cdot \left[\int_{-\infty}^{\infty}\left\{\int_{-\infty}^{\infty} g(x)\exp(-j2\pi f x)\, dx\right\}\right. \\ &\quad \left. \cdot\ \exp(j2\pi f I_b) J_k(r) J_n(r)\, df\right]^2 \\ &= 2(-1)^{k+n}\left[\int_{-\infty}^{\infty} g(x)F(x)\, dx\right]^2 \end{aligned} \quad (9)$$

where

$$\begin{aligned} F(x) &= \int_{-\infty}^{\infty} \exp(-j2\pi f(x - I_b)) J_k(r) J_n(r)\, df \\ &= \begin{cases} -2j\displaystyle\int_0^{\infty} \sin[2\pi f(x - I_b) J_k(r) J_n(r)\, df \\ \quad k \pm n \text{ isodd} \\ 2\displaystyle\int_0^{\infty} \cos[2\pi f(x - I_b)] J_k(r) J_n(r)\, df \\ \quad k \pm n \text{ is even.} \end{cases} \end{aligned} \quad (10)$$

Equation (10) cannot be numerically integrated because the re-

sult of integrating the product of higher order Bessel functions $(k, n \geq 1)$ from zero to infinite does not converge. Therefore, further manipulations on (9) is needed.

In (10), we first consider the case when $k \pm n$ is odd

$$\begin{aligned} F(x) &= \frac{-j}{\pi I_m} \int_0^{\infty} \sin\left[\frac{r}{I_m}(x - I_b)\right] J_k(r) J_n(r)\, dr \\ &= \frac{-j}{\pi I_m} \int_0^{\infty} \sin\left[\frac{r}{I_m}(x - I_b)\right] \\ &\quad \cdot \left\{ \frac{2}{\pi} \int_0^{\pi/2} J_{k+n}(2r\cos(\theta)) \cos[(k-n)\theta]\, d\theta \right\} dr \\ &= \frac{-2j}{\pi^2 I_m} \int_0^{\pi/2} \cos[v\theta] \\ &\quad \cdot \left\{ \int_0^{\infty} \sin\left[\frac{r}{I_m}(x - I_b)\right] J_{\mu}(ar)\, dr \right\} d\theta \end{aligned} \tag{11}$$

where

$$\begin{aligned} \mu &= k + n \quad \text{(odd number)} \\ v &= |k - n| \\ a &= 2\cos(\theta). \end{aligned} \tag{12}$$

By substituting (11) into (9)

$$\begin{aligned} &\int_{-\infty}^{\infty} g(x) F(x)\, dx \\ &\quad = \frac{-2j}{\pi^2 I_m} \int_0^{\pi/2} \cos[v\theta] \\ &\qquad \cdot \left\{ \int_{I_b - aI_m}^{I_b + aI_m} g(x) \frac{\sin\left[\mu \sin^{-1}\left(\dfrac{b}{a}\right)\right]}{\sqrt{a^2 - b^2}}\, dx \right\} d\theta \end{aligned} \tag{13}$$

where $b = (x - I_b)/I_m$. Assuming that

$$\begin{aligned} \sin(\lambda) &= \frac{b}{a} \\ x &= I_b + aI_m \sin(\lambda) \\ dx &= I_m \sqrt{a^2 - b^2}\, d\lambda \end{aligned} \tag{14}$$

then (13) becomes

$$\begin{aligned} &\int_{-\infty}^{\infty} g(x) F(x)\, dx \\ &\quad = \frac{-2j}{\pi^2} \int_0^{\pi/2} \cos[v\theta] \\ &\qquad \cdot \left\{ \int_{-\pi/2}^{\pi/2} g(I_b + aI_m \sin(\lambda)) \sin(\mu\lambda)\, d\lambda \right\} d\theta. \end{aligned} \tag{15}$$

Therefore, for the case when $k \pm n$ is odd, the general expression of mean square current at a frequency $k\omega_1 \pm n\omega_2$ can be obtained by substituting (15) into (9), and the final result is given by

$$\begin{aligned} \langle i^2_{k\omega_1 \pm n\omega_2} \rangle = \frac{8}{\pi^4} \Bigg[\int_0^{\pi/2} \cos[v\theta] \Bigg\{ \int_{-(\pi/2)}^{\pi/2} g(I_b + aI_m \sin(\lambda)) \\ \cdot \sin(\mu\lambda)\, d\lambda \Bigg\} d\theta \Bigg]^2. \end{aligned} \tag{16}$$

The bounded integration limits in (16) enable one to numerically calculate the mean square current at $k\omega_1 \pm n\omega_2$ where $k \pm n$ is odd. In other words, the fundamental output signal power and odd-order IM product power resulted from modulating a laser (whose L-I transfer function is $g(x)$) by two tones at ω_1 and ω_2 can all be calculated from (16). Following the same derivation procedure, we can obtain the general expression of $\langle i^2_{k\omega_1 \pm n\omega_2} \rangle$ when $k \pm n$ is even

$$\begin{aligned} \langle i^2_{k\omega_1 \pm n\omega_2} \rangle = \frac{8}{\pi^4} \Bigg[\int_0^{\pi/2} \cos[v\theta] \Bigg\{ \int_{-(\pi/2)}^{\pi/2} g(I_b + aI_m \sin(\lambda)) \\ \cdot \cos(\mu\lambda)\, d\lambda \Bigg\} d\theta \Bigg]^2. \end{aligned} \tag{17}$$

Note that (16) and (17) are also applicable to the case of external modulations if $g(x)$ is used to represent the L-V transfer function of an external-modulator-based optical transmitter and the modulating current signal $I(t)$ is replaced by the corresponding modulating voltage signal $V(t)$.

B. Analysis of Large-Signal SFDR

According to its definition, SFDR is equal to CNR and C/IM$_3$ as follows:

$$\text{SFDR} = \frac{\langle i_C^2 \rangle}{\langle i_N^2 \rangle \cdot BW} = \frac{\langle i_C^2 \rangle}{\langle i_{\text{IM}_3}^2 \rangle} \tag{18}$$

where BW is the signal bandwidth. According to (16)

$$\begin{aligned} \langle i_C^2 \rangle = \frac{8}{\pi^4} \Bigg[\int_0^{\pi/2} \cos[\theta] \Bigg\{ \int_{-(\pi/2)}^{\pi/2} g(I_b + aI_m \sin(\lambda)) \\ \cdot \sin(\lambda)\, d\lambda \Bigg\} d\theta \Bigg]^2 \end{aligned} \tag{19}$$

$$\begin{aligned} \langle i_{\text{IM}_3}^2 \rangle = \frac{8}{\pi^4} \Bigg[\int_0^{\pi/2} \cos[\theta] \Bigg\{ \int_{-(\pi/2)}^{\pi/2} g(I_b + aI_m \sin(\lambda)) \\ \cdot \sin(3\lambda)\, d\theta \Bigg\} d\theta \Bigg]^2. \end{aligned} \tag{20}$$

The total mean square noise current $\langle i_N^2 \rangle$ includes RIN noise, shot noise, and receiver thermal noise. Note that, once the noise floor $\langle i_N^2 \rangle \cdot BW$ is specified, only a single value of OMI/carrier satisfies the equation of CNR = C/IM$_3$. By substituting this particular OMI/carrier into the CNR calculation, the corresponding SFDR can be obtained. In other words, once OMI/carrier is fixed, the SFDR is fixed. This condition is very different from the small-signal SFDR which is independent of OMI/carrier. This important point is illustrated in Fig. 1 (where P_{in} and P_{out} are the input and output RF/microwave power, and SFDR$_{\text{norm}}$ is equal to CNR per Hz$^{2/3}$), from which we can see that the small-signal SFDR$_{\text{s}}$ can be easily estimated from the normalized SFDR$_{\text{norm}}$ based on the relationship SFDR$_{\text{s}}$ = SFDR$_{\text{norm}}$ + $(2/3)10\ \log(\text{BW}_2)$, without knowing the OMI/carrier or the device transfer function $g(x)$. On the other hand, the large-signal SFDR$_l$ can be estimated only if the OMI/carrier and $g(x)$ are both known.

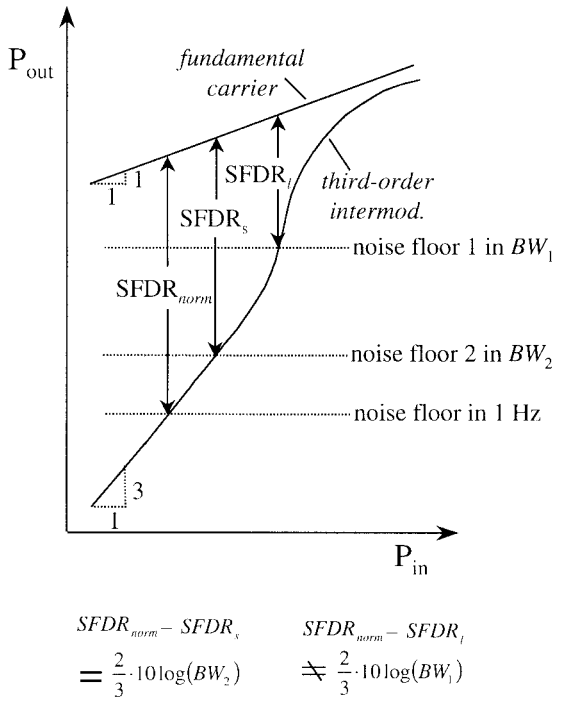

Fig. 1. A conceptual diagram illustrating large-signal SFDR with noise floor 1 in bandwidth BW1 (SFDR_l), small-signal SFDR with a noise floor 2 in bandwidth BW_2 (SFDR_s), and SFDR in a normalized 1 Hz bandwidth ($\mathrm{SFDR}_{\mathrm{norm}}$).

The above concept can be further explained to get a better insight understanding as follows. From Fig. 1, once a small-signal SFDR at a certain input RF or microwave driving power is given, we can estimate not only the total noise per hertz, but also the *constant* third-order coefficient of the Taylor series expansion of the LD or external modulator transfer function. We can then use the third-order Taylor series coefficient to predict the IM_3 for any other input RF/microwave power. However, a large-signal SFDR is obtained only when OMI/carrier, the center frequency (f_c) of a narrow-band signal, and $g(x)$ are all given. Therefore, a large-signal SFDR not only can provide information about the noise floor $\langle i_N^2 \rangle \cdot BW$, but also a Taylor series whose coefficients are OMI/carrier and f_c-dependent.

Equation (18) can be used to obtain the static-clipping limited large-signal SFDR for both a LD and an external modulator. However, in the case of an LD, SFDR due to (1) dynamic clipping [20]–[24] or (2) laser relaxation oscillation can become predominant. SFDR due to dynamic clipping can be obtained from (16) and (17) as long as the L-I transfer function $g(x)$ due to dynamic clipping can be measured, as will be demonstrated in Section IV. SFDR due to laser relaxation oscillation can be approximately estimated according to [2]

$$\mathrm{SFDR} \approx \frac{2}{3} \cdot 10 \log \left[\frac{I_D^2 \Big/ \left| \left(\frac{f_c}{f_r} \right)^4 - \frac{1}{2} \left(\frac{f_c}{f_r} \right)^2 \right|}{\langle i_N^2 \rangle} \right] \tag{21}$$

where I_d is the detected photocurrent, f_r is the relaxation oscillation frequency of semiconductor LD, and f_c is the center frequency of the two modulating carriers. Whether static clipping, dynamic clipping, or relaxation oscillation becomes the dominant factor in determining the final large-signal SFDR depends on the OMI/carrier, f_r, f_c, and the intrinsic linearity characteristics of the L-I or L-V curve.

III. Comparing IM_n Products from Analysis and Computer Simulation

Computer simulations were carried out to verify (16) and (17) by using two transfer functions $g(x)$. One is the ideal laser L-I curve and the other is the ideal L-V curve of an external modulator, which are shown in the insets of Figs. 2 and 3, respectively. In our simulations, the phases of the two tones were assumed to be random, and the resultant $\mathrm{IM_n}$ products were obtained by averaging over 20 000 times with respect to the fast-Fourier-transformed (FFT) spurious frequency components. The results are shown in Figs. 2 and 3, for the cases of ideal L-I and L-V, respectively. We can see that the analytical results match the simulation results almost exactly for $0.51 \leq$ OMI/carrier ≤ 0.6, and the match also holds for OMI/carrier > 0.6 (not shown). Note that all even order NLD's are zero for an ideal L-V transfer function whose bias is at its inflection point, as expected.

From Figs. 2 and 3, we note that when OMI/carrier >0.51, the lower order NLD's, i.e., the second- or third-order NLD's, are more critical than higher order NLD's. This observation can be compared with the spectral analysis results for an ideal L-I curve when there are multiple equal-amplitude channels [7]. In that case, the second- and third-order NLD's become dominant only when the total root-mean-square (rms) OMI is greater than about 0.45. In a typical downstream CATV LD which transports multiple equal-amplitude AM-VSB channels, the total rms OMI due to AM channels usually is about from 0.25 to 0.3, and the dominant NLD's for an ideal L-I curve are the fifth- or sixth-order.

From our results given in Figs. 2 and 3, therefore, a third-order predistortion circuit should be very helpful to increase the dynamic range of an ideal LD which is used to transport multiple unequal-amplitude signals within a narrowband. We will see later in Section V that even when the laser is nonideal, the resultant NLD's are the same as those given in Fig. 2 when strong clipping due to narrow-band signals takes place (when OMI/carrier >0.6).

It can also be observed from Figs. 2 and 3 that the difference between $\mathrm{C/IM_3}$ due to ideal laser L-I and ideal external modulator L-V is about 6 dB, as summarized in Fig. 4. The main reason is that the latter is a two-sided limiter, while the former is a one-sided limiter. This 6 dB difference has also be observed in the case of multiple equal-amplitude channels [8]. Also shown in Fig. 4 is the analytical (or simulation) $\mathrm{C/IM_3}$ results for several other transfer functions of external modulators (as illustrated in Fig. 5), including those for a conventional Mach–Zehnder interferometer (MZI) modulator, an MZI modulator with a perfect arcsine predistorter, and an MZI modulator with a third- and fifth-order arcsine predistorter [8]. In Fig. 4, the performance of $\mathrm{C/IM_3}$ (in the

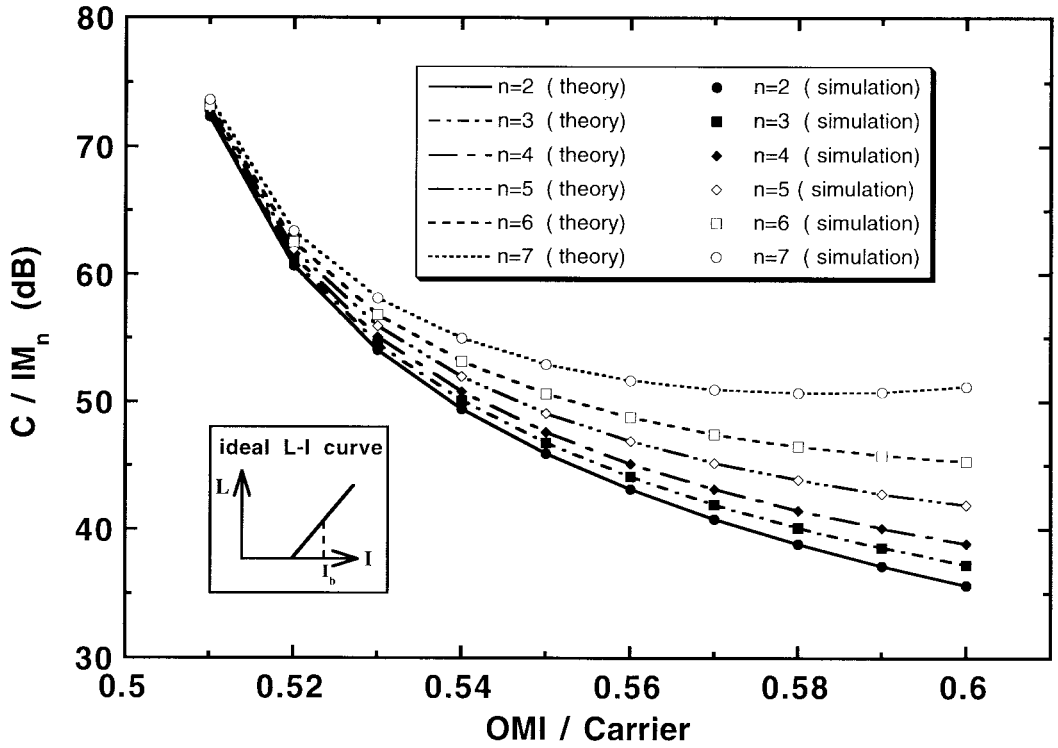

Fig. 2. C/IM$_n$ versus OMI/carrier for an ideal laser diode (with an L-I curve shown in the inset) from calculation (lines) and computer simulation (symbols). The subscript n indicates the order of nonlinearity.

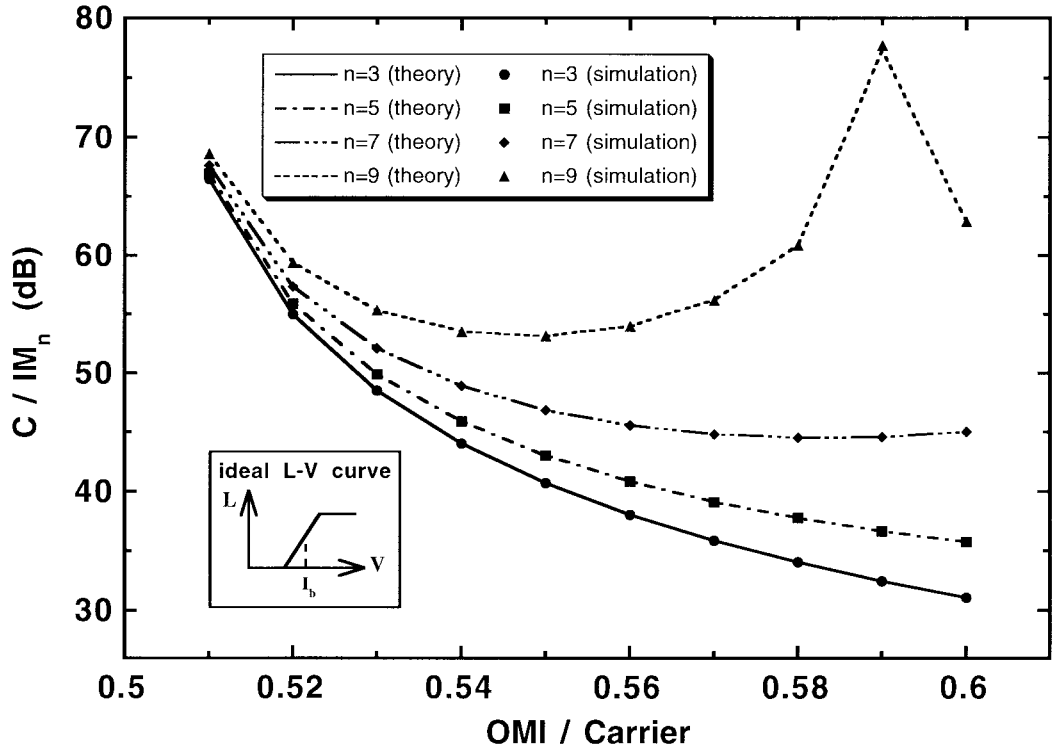

Fig. 3. C/IM$_n$ versus OMI/carrier for an ideal external modulator (with an L-V transfer function shown in the inset) from calculation (lines) and computer simulation (symbols). The subscript n indicates the order of nonlinearity.

range of OMI/carrier $>$0.508) from the best to the worst is in the following sequence: ideal external modulator, MZI with a third- and fifth-order arcsine predistorter, MZI without predistorter, and MZI with perfect arcsine predistorter. Note MZI with a third- and fifth-order arcsine predistorter and MZI without predistorter are intrinsically nonlinear under small-signal modulations, hence C/IM$_3$ have finite values even OMI/carrier is in the small-signal region.

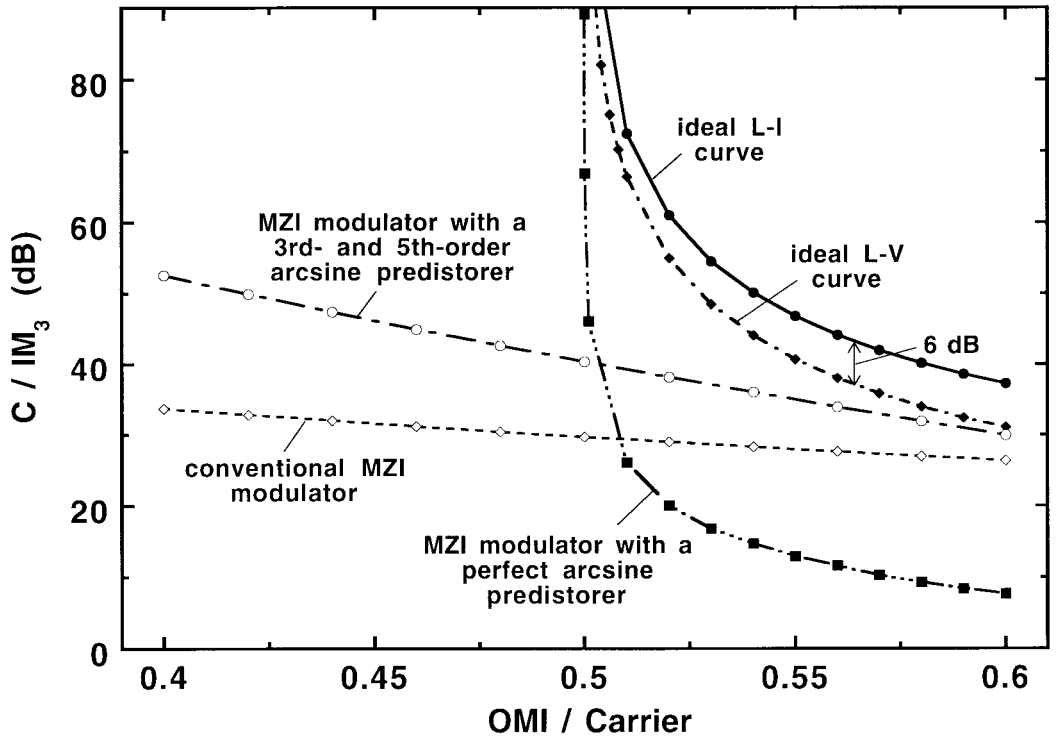

Fig. 4. C/IM_3 versus OMI/carrier performances for an ideal LD L-I curve, and external modulators with various linearization techniques.

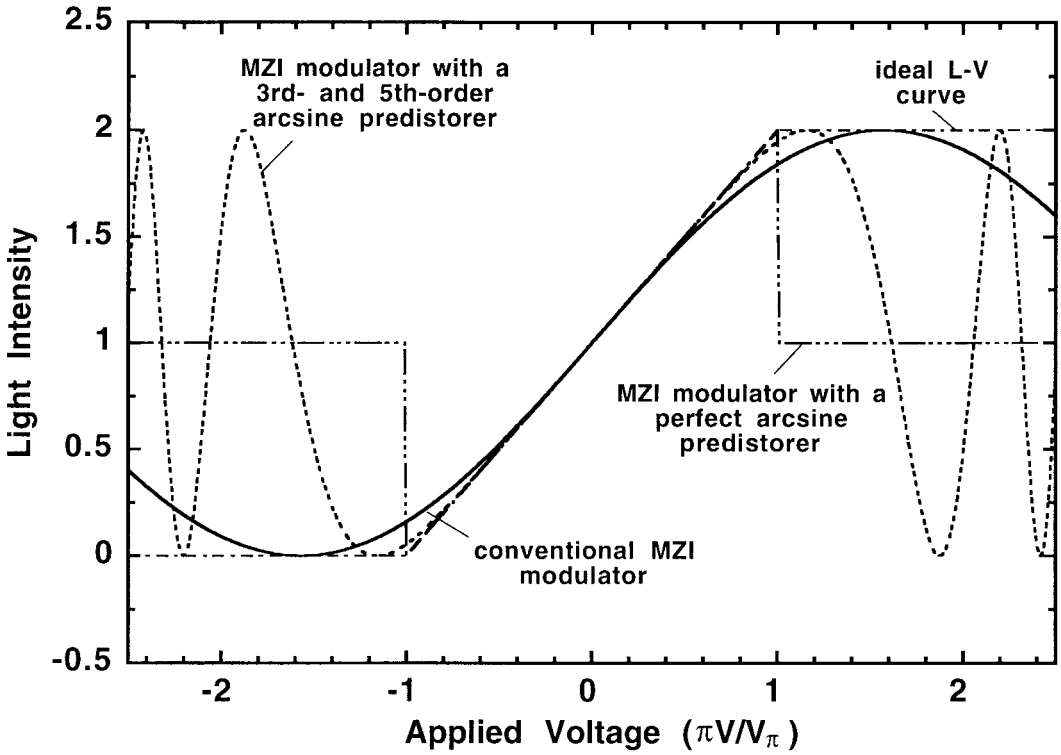

Fig. 5. Transfer functions of a conventional MZI modulator, an MZI modulator with a perfect arcsine predistorter, an MZI modulator with a third- and fifth-order arcsine predistorter, and an ideal external modulator.

IV. Measurement of L-I Curve for a LD Under Dynamic Clipping

The L-I curve for a LD under dynamic clipping is obtained by comparing the output and input waveforms when a sinusoidal modulating signal has an OMI slightly greater than 1.0. An example is illustrated in Fig. 6. Fig. 6(a) shows the input waveform of a 307.2625 MHz signal (dashed curve) and the corresponding LD output waveform (solid curve) when OMI $\approx$1.0. It can be seen that, when compared with the input

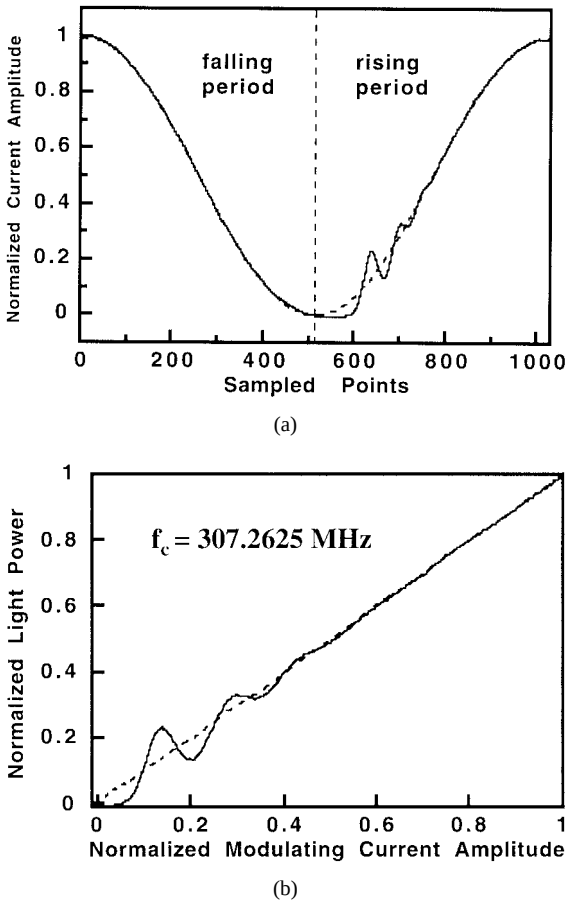

Fig. 6. (a) One cycle of measured (normalized) optical time response for a sinusoidal modulating current of frequency 307.2625 MHz and peak OMI of 1.0. The dotted and the solid lines illustrate the modulating carrier and the measured optical intensity output, respectively. (b) Dynamically clipped L-I curve (normalized) obtained from Fig. 6(a). The solid and dotted lines are converted from the rising and falling periods in Fig. 6(a), respectively.

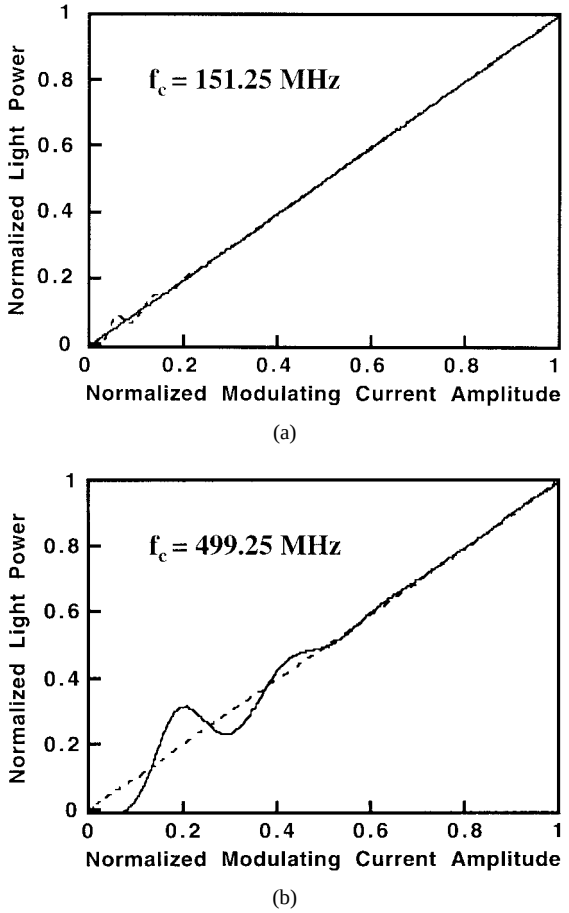

Fig. 7. The dynamically clipped L-I curves for a sinusoidal modulating current with a frequency of (a) 151.25 MHz and (b) 499.25 MHz, each has a peak OMI of 1.0.

waveform, the output waveform has a clear turn-on delay in the rising period, and a very small amplitude compression at the lower edge of the falling period. Note that in Fig. 6(a), the input and output waveforms were carefully adjusted to be in-phase and are curve-fitted with respect to each other via a minimum-mean-square-error (MMSE) algorithm. The oscillating portion in the second-half cycle is related to the relaxation oscillation frequency of the semiconductor laser. By normalizing the output waveform with respect to the input waveform, the normalized L-I curves for the rising and falling periods can then be separately obtained, and are shown by solid and dashed curves in Fig. 6(b), respectively. Note also that the normalized L-I curves obtained in these two periods are different when clipping occurs, but are the same when clipping does not occur. Since the spurious IM products are the average results of the IM products generated from each L-I curve, the resultant nth order IM_n products can be written as follows:

$$\mathrm{IM}_n = \frac{1}{2} \cdot \mathrm{IM}_{n,\text{falling period}} + \frac{1}{2} \cdot \mathrm{IM}_{n,\text{rising period}} \quad (22)$$

where IM_n is calculated by substituting the measured dynamically clipped L-I curve (as the function $g(x)$) into (16) and (17).

A normalized dynamically clipped L-I curve such as the one in Fig. 6(b), however, is dependent on the frequency of the modulating signal. When a large-signal SFDR for narrow-band signals is to be estimated, the center frequency of the two closely spaced modulating tones can be used to measure the L-I curves. To show that the dynamically clipped L-I curves are indeed frequency-dependent, we use two other frequencies, i.e., 151.25 and 499.25 MHz, each with a peak OMI $\approx$1.0, to obtain different L-I curves as shown in Fig. 7(a) and (b), respectively. We can see that when the frequency of the modulating tone increases, the zero output light region (proportional to the turn-on delay) increases, and the undulation of the L-I curve (due to laser relaxation oscillation) becomes looser.

V. Comparing the Measured and Calculated IM_n Products of a Clipped-LD

We carried out a $\mathrm{C/IM_3}$ measurement by using a typical CATV-quality distributed feedback (DFB) laser which can be used to transport 80 AM-VSB channels with standard performance. The laser threshold and bias currents were 8.9 and 23.5 mA, respectively. We used two tones at 169.25 and 193.25 MHz to measure the $\mathrm{C/IM_3}$ when the laser is operated in weak and strong clipping regimes. We also used a single

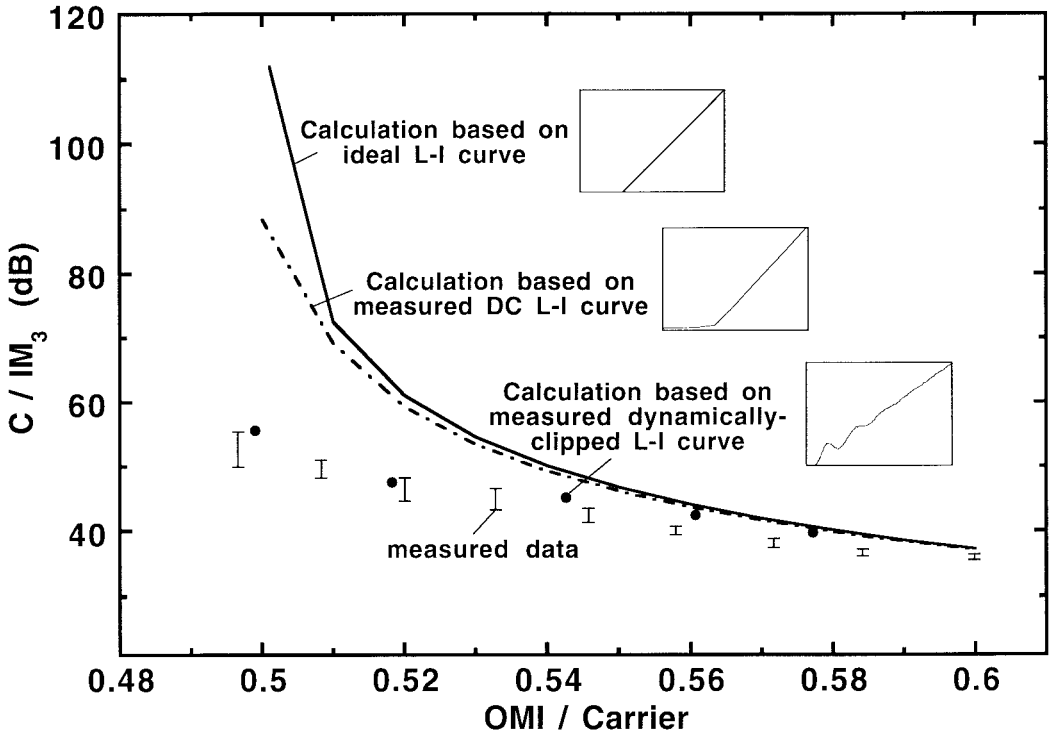

Fig. 8. C/IM_3 versus OMI/carrier for a directly modulated laser diode. Shown in the figure are calculated results based on ideal L-I curve (line), measured DC L-I curve (dash-dot), and measured dynamically clipped L-I curve (solid circles). Bars represent the measured data.

tone at 181.25 MHz to measure the dynamically clipped L-I curves for various OMI values. The measured dynamically clipped L-I curves are then plugged into $g(x)$ in (16) so that we can obtain calculated results. Fig. 8 shows the measured (bars) and calculated (solid circles) C/IM_3 values. We can see that the differences between the measured and calculated results are within 3–4 dB. Also shown in Fig. 8 are the calculated C/IM_3 values based on an ideal L-I curve and the measured conventional dc L-I curve, respectively. We can see that when OMI/carrier is smaller than about 0.6, both the ideal L-I curve and the measured dc L-I curve can result in C/IM_3 values over-optimistic by up to 36 dB at OMI/carrier $\approx$0.5. Whereas when OMI/carrier is greater than about 0.6, there is essentially no difference among the calculated values based on the ideal L-I curve, the measured dc L-I curve, and the measured dynamically clipped L-I curve. What this implies is that the dynamic-clipping-induced NLD's dominate when a laser is weakly clipped, while static-clipping-induced NLD's dominate if a laser is strongly clipped.

Note that the measured relaxation oscillation frequency of the semiconductor LD we used was around 8.5 GHz. With this high relaxation oscillation frequency, the C/IM_3 values based on rate equations [2], [21] can be estimated to be much higher than those shown in Fig. 8 when OMI/carrier $>$0.51. Therefore, in the clipping region with OMI/carrier $>$0.51, IM_3 products due to laser relaxation oscillations can be neglected even though the modulating tone sees a significant undulation in the dynamically clipped L-I curve (Figs. 6 and 7).

Now we know that dynamic clipping plays an important role in the weak clipping region (especially when OMI/carrier is close to 0.5). We also know that the dynamically clipped L-I curves are frequency-dependent, as shown in Figs. 6(b), and 7(a) and (b). It is therefore worthwhile to check if our theoretical model can match measured weak-clipping-induced NLD's due to narrow-band modulating signals in different frequency regions. To verify this point, we used three sets of narrow-band modulating carriers, i.e., (139.25,163.25), (295.2625, 319.2625), and (487.25,511.25) MHz, with OMI/carrier $\approx$0.5, to carry out the second- to eigth-order IM product measurement. The reason why we pick OMI/carrier $\approx$0.5 is because dynamic-clipping induced NLD's dominate over those due to other mechanisms by a very large magnitude, as was shown in Fig. 8. The results are shown in Fig. 9(a)–(c) for the three different frequency sets, respectively. We can see that the measured and calculated data match fairly well. The 3–5 dB differences are mainly due to the difficulty in setting the OMI/carrier precisely at 0.5. In our measurement, we find that the unavoidable power level variation of $\pm$0.2 dB for each modulating carrier, which corresponds to a variation of OMI from 0.5 to 0.5 $\pm$ 0.01, can result in 3–8 and 1–4 dB power variations in the measured IM_2 and IM_3, respectively. This result of measurement uncertainty can also be observed from the solid circles in Fig. 8 that when OMI/carrier changes from 0.5 to 0.51, the resultant C/IM_3 can change by about 5 dB. Other measurement uncertainties are due to 1) the amplitude accuracy in measuring the optical time response such as the one given in Fig. 6(a), 2) the slight misalignment of amplitude and phase due to MMSE algorithm in generating the dynamically clipped L-I curve, and 3) the random variations in the power levels of IM products.

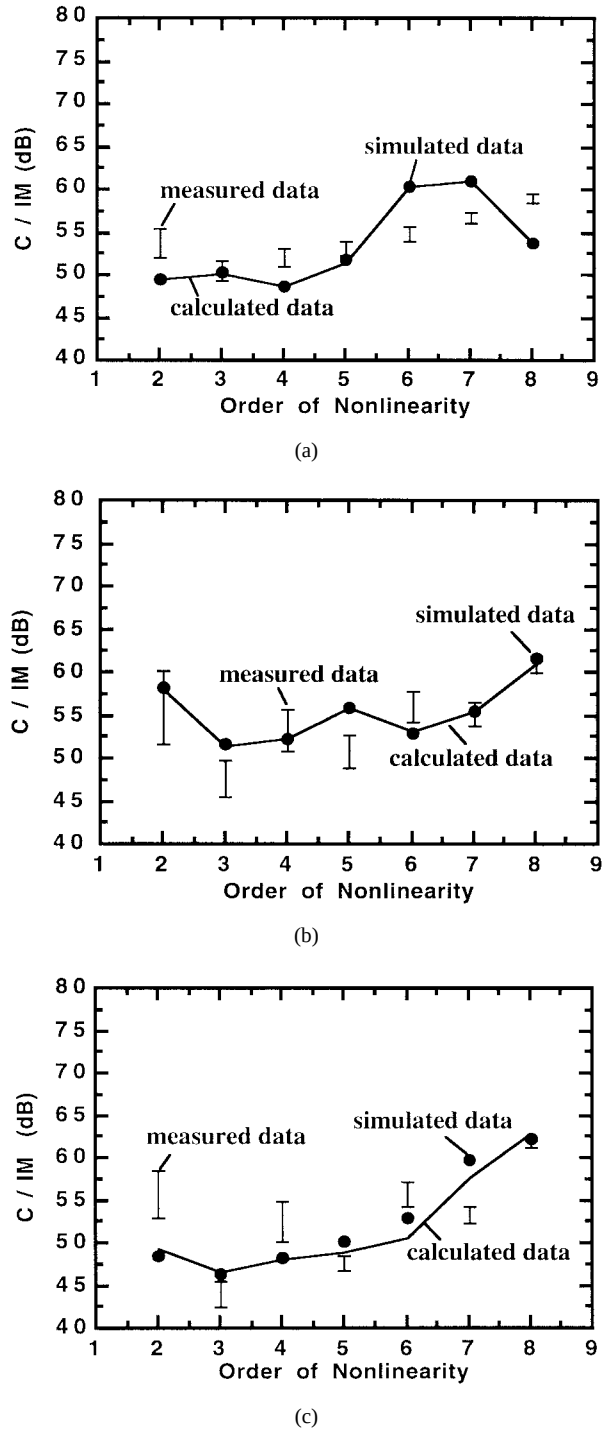

Fig. 9. C/IM versus orders of nonlinearity for three sets of two-tone carriers: (a) (139.25,163.25) MHz, (b) (295.2 625 319.2625) MHz, and (c) (487.25, 511.25) MHz, with OMI/carrier $\approx$0.5. The solid circles, solid lines and bars correspond to simulated, calculated and measured results, respectively.

It should be noted that the lower order IM products (e.g., second and third) are more severe than higher order IM products. Since ideal L-I curve also gives lower order dominant IM products (see Fig. 2), we conclude that for OMI from slightly less than 0.5 to much higher than 0.5, it is always the lower order IM products dominate. Therefore, in estimating SFDR for narrow-band modulating signals, we only have to consider C/IM_3.

VI. SFDR Due to Dynamic/Static Clipping in LD and Static Clipping in External Modulator

In Sections III–V, we have concentrated on investigating the IM products due to clipping effects. In this section, we will investigate the theoretical upper-bound for large-signal SFDR due to static clipping in an ideal LD and an ideal external modulator, and will show the SFDR reduction due to LD dynamic clipping.

As described in Section II-B, when the transfer function $g(x)$ and the system noise floor are both known, the large-signal SFDR and the corresponding optimum OMI/carrier can be obtained from (18). Using this fact, we calculated the SFDR's and the corresponding optimum OMI/carrier for an ideal LD L-I curve and an ideal external modulator L-V curve, and results are given in Fig. 10. All the points in Fig. 10 were calculated based on a noise floor $(=\langle i_N^2\rangle \cdot BW)$ ranging from 7.4×10^{-16} to 1.0×10^{-9} A^2. These noise floors correspond to a signal bandwidth of 1 MHz, a received photocurrent of 1 mA, a thermal noise current density of 10 $pA/\sqrt{Hz}$, and a RIN noise ranging from -155 to -95 dB/Hz. We can observe that the SFDR of an ideal LD is always better than that of an ideal external modulator by 5–7 dB. However, when we consider the LD dynamic clipping which practically exists, the ideal LD static SFDR performance is degraded significantly for OMI/carrier $>$0.6. Note also that the SFDR's for the ideal LD and the ideal external modulator approach infinite when OMI/carrier is close to 0.5 because of the perfect (one-sided or two-sided) limiter characteristics. On the other hand, when we consider a dynamically clipped L-I curve, the clipping occurs even when OMI/carrier is smaller than 0.5 because of the slight bending of the L-I curve near its knee (see Figs. 6(b) and 7).

Calculated SFDR's for the MZI modulators with various linearization techniques (whose transfer functions were given in Fig. 5) are shown in Fig. 11. The values of the noise floor are the same as those used for Fig. 10. It is interesting to see that, when using conventional MZI modulator as an example, the largest large-signal SFDR based on our analysis corresponds to the small-signal SFDR by using conventional method [2]. We also note that those L-V curves with a perfectly linear center region such as an ideal external modulator and an MZI modulator with a perfect arcsine predistorter (see Fig. 5) has their SFDR's approaching infinite when OMI/carrier is close to 0.5.

If we plot the SFDR of a dynamically clipped LD also on Fig. 11, as shown by dotted lines, we can find a very informative comparison as follows. First of all, we note that for a device with a better linearity, its IM_3 versus OMI/carrier curve will intersect with a given system noise floor at a higher optimum OMI/carrier where the corresponding SFDR is obtained. Now if we compare the optimum OMI/carrier along the same noise floor (i.e., the contour lines in Fig. 11) for various devices, we can see that a typical CATV-quality LD exhibits a higher OMI/carrier than that of a MZI modulator with a third- and fifth-order arcsine predistorter. This implies that the linearity of a dynamically clipped LD is better than that of a commercial MZI modulator which uses a third- and fifth-order arcsine predistorter.

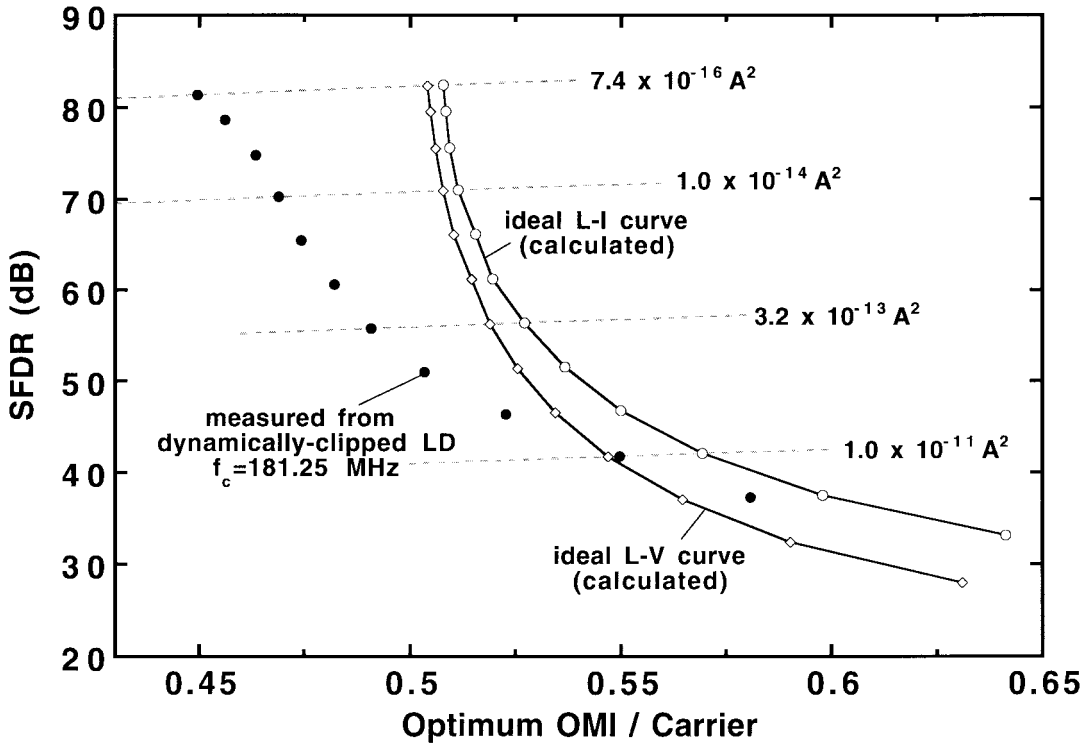

Fig. 10. Comparing SFDR versus OMI/carrier for ideal L-I curve (open circles), ideal L-V curve (open diamonds), and dynamically clipped L-I curve (solid circles). Solid circles were measured based on a dynamically clipped LD and two modulating tones centered at 181.25 MHz. The dashed lines represent the contours of mean square current noise floor.

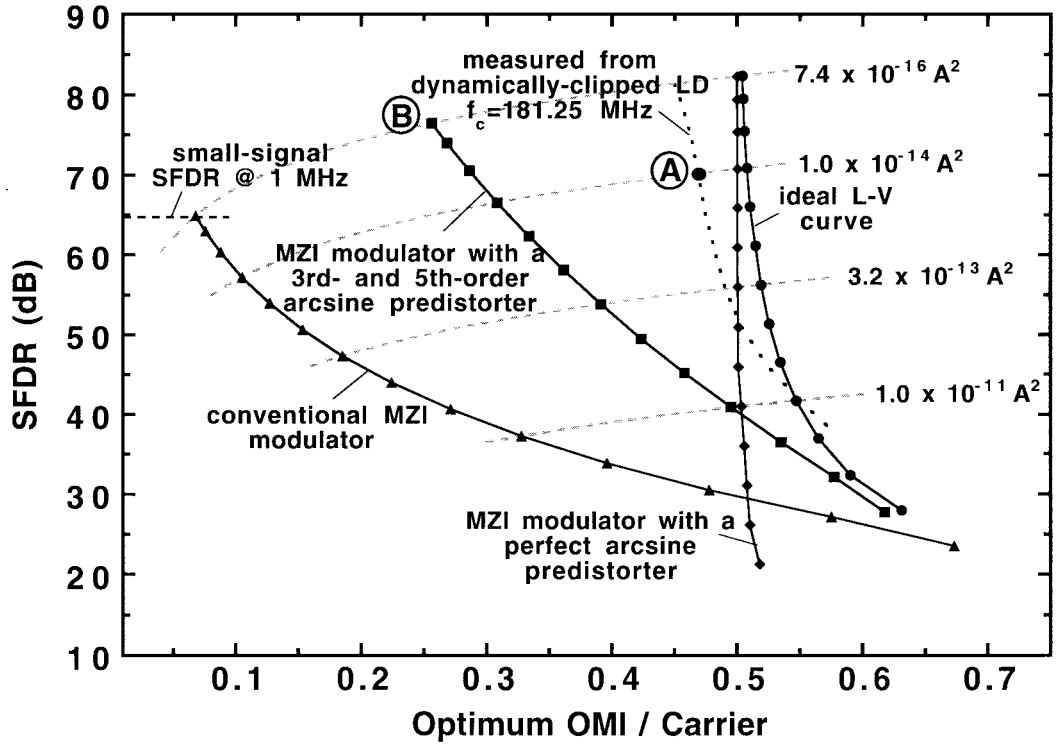

Fig. 11. Comparing SFDR versus OMI/carrier for MZI modulators with various linearization techniques. All data except the dotted line are based on calculations. The dashed lines represent the contours of mean-square current noise floor.

However, direct- and external-modulation systems may have different system noise floors. Therefore, their SFDR's must not be compared on the same contour line in Figs. 10 or 11. For example, assuming that the RIN noise of an externally and a directly modulated system are -155 dB/Hz (noise floor $= 7.4 \times 10^{-16}$) and -140 dB/Hz (noise floor $= 1.0 \times 10^{-14}$),

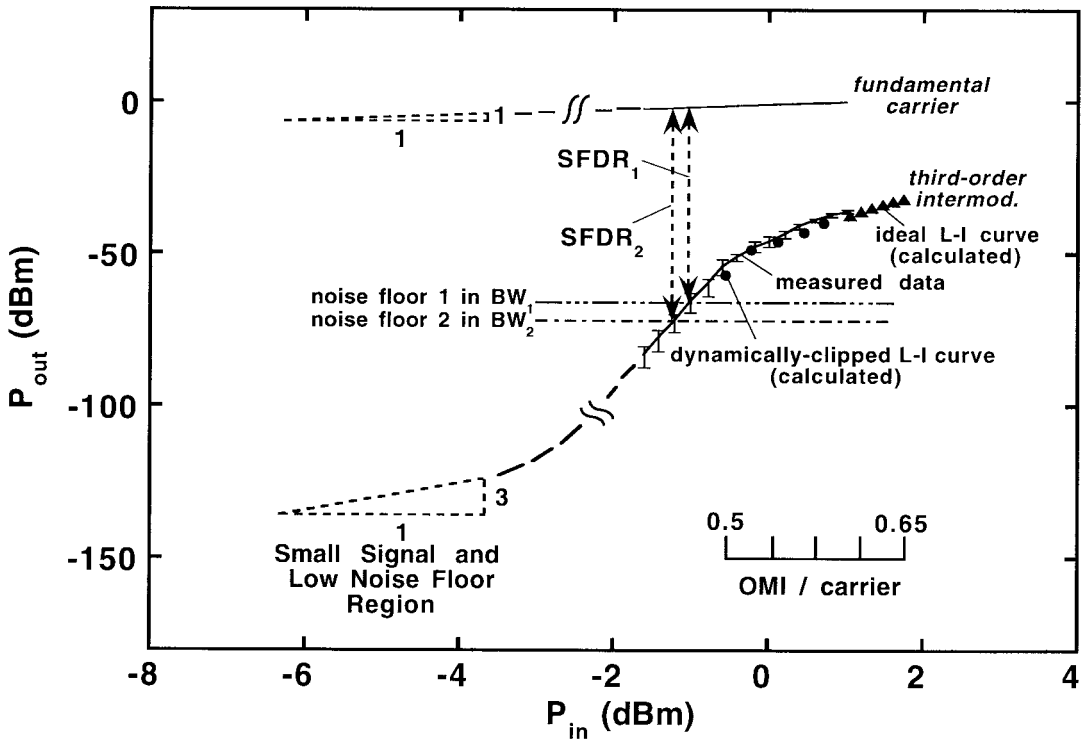

Fig. 12. Demonstrating the concept shown in Fig. 1 by actual measurement and calculations. It can be seen that the third-order intermod in the region of OMI/carrier close to 0.5 does not follow the conventional 1:3 growth rate, and can be predicted by using our analysis. The conventional 1:3 region is apparently for small modulating signals and low noise floors. BW_1 and BW_2 differ by a factor of four.

respectively. The corresponding SFDR's for a dynamically clipped LD and an MZI modulator with a third- and fifth-order arcsine predistorter are 70.1 dB (point A) and 76.5 dB (point B), respectively. Therefore, the latter exhibits a better SFDR, even though its liinearity is inferior to the former.

VII. Discussions

The concept of large-signal SFDR illustrated in Fig. 1 can now be demonstrated in terms of measured and analytical results. In Fig. 12, we can use our analytical model [(18)] to predict how large the IM_3 products are when OMI/carrier is close to 0.5. Calculated results for the ideal LD L-I curve and the dynamically clipped L-I curves are shown by solid triangles and circles, respectively (note the dynamically clipped L-I curve is measured by using a 181.25 MHz tone). The measured results are based on two modulating tones at 169.2 and 193.25 MHz. Once again, we can see that the measured data match the calculated data fairly well.

In Fig. 12, we see that when OMI/carrier is near 0.5, IM_3 increases much faster than the conventional 3:1 rate (for every 1 dB increase in the fundamental carrier, there is a 3 dB increase in IM_3). But IM_3 also gradually saturates when P_{in} increases to a very large level. As was explained in the conceptual diagram Fig. 1, the difference between two arbitrary SFDR's in the large-signal region cannot be related by $(2/3)\cdot 10\log(BW_1/BW_2)$. This is shown in Fig. 12, in which the difference between $SFDR_1$ and $SFDR_2$ (whose noise bandwidths differ by a factor of four) is $\sim$6 dB, rather than the 4 dB predicted by the above formulae.

Note that the varying slope is due to the fact that the third-order coefficient in the Taylor series expansion is OMI-dependent, as explained earlier. Another fact in Fig. 12 we should point out is that when the modulating signal becomes too large, it is always the static clipping that dominates. This fact was already mentioned when we discussed Fig. 8.

VIII. Conclusion

In this paper, we have investigated the large-signal two-tone SFDR (OMI/carrier near 0.5) due to dynamic/static clipping in LD and static clipping in external modulator. We have derived the closed-form formulae, (16)–(18), which are useful for arbitrarily shaped L-I or L-V transfer functions. In the case of ideal static clipping, a noise floor ranging from 7.4×10^{-16} to $1.0\times 10^{-9}A^2$ and OMI/carrier $>$0.5, we observe that the SFDR of an ideal LD is always better than that of an ideal external modulator by 5–7 dB. However, in the case when a realistic LD with dynamic clipping is considered, the ideal LD static SFDR performance is degraded significantly when OMI/carrier $<$0.6. In other words, dynamic-clipping-induced NLD's dominate when a laser is weakly clipped (e.g., OMI/carrier is in the vicinity of 0.5), while static-clipping-induced NLD's dominate if a laser is strongly clipped (e.g., OMI/carrier $>$0.6). The effects of LD static and dynamic clippings were both confirmed by measuring the dynamically clipped L-I curve and the corresponding NLD's of a typical CATV-quality DFB LD. Through analysis and measurement, we can clearly see that a large-signal SFDR depends on not only the transfer functions, but also on OMI/carrier. This fact is very different from the conventional small-signal SFDR.

It should also be noted that the large-signal SFDR for a LD under dynamic clipping depends further on modulating signal frequency, which restricts the applicability of our SFDR results to narrow-band signals.

We have also used our theoretical model to predict the NLD's arising from the MZI modulators with various linearization techniques. By comparing the large-signal third-order intermodulation products of LD's and external modulators, we see that even though dynamic clipping significantly degrades the linearity of a LD, a typical CATV-quality LD can still exhibit a better linearity than that of a MZI modulator with a third- and fifth-order arcsine predistorter. However, the SFDR comparison between these two devices can only be made when the system noise floor is known.

REFERENCES

[1] C. Cox, III, E. Ackerman, R. Helkey, and G. E. Betts, "Techniques and performance of intensity-modulation direct-detection analog optical links," *IEEE Trans. Microwave Theory Tech.*, vol. 45, pp. 1375–1383, Aug. 1997.

[2] W. I. Way, "Optical fiber-based microcellular systems: An overview," *IEICE Trans. Commun.*, vol. E76-B, no. 9, pp. 1091–1102, Sept. 1993.

[3] W. B. Bridges and J. H. Schaffner, "Distortion in linearized electrooptic modulators," *IEEE Trans. Microwave Theory Tech.*, vol. 43, pp. 2184–2197, Sept. 1995.

[4] J. H. Schaffner and W. B. Bridges, "Intermodulation distortion in high dynamic range microwave fiber-optic links with linearized modulators," *J. Lightwave Technol.*, vol. 11, pp. 3–6, Jan. 1993.

[5] W. I. Way, K. Y. Yen, and W. W. Deng, "Super-FM and analog-to-digital conversion technologies for next-generation wireless access in optical fibers," *Optical Quantum Electron.*, vol. 28, pp. 1521–1534, 1996.

[6] K. Kim, "Analog-to-digital conversion and harmonic noise due to the integral nonlinearity," *IEEE Trans. Instrum. Measurement*, vol. 43, Apr. 1994.

[7] P. Y. Chiang and W. I. Way, "Ultimate capacity of a laser diode in transporting multichannel M-QAM signals," *J. Lightwave Technol.*, vol. 15, pp. 1914–1924, Oct. 1997.

[8] D. A. Atlas, "On the modulation limit in externally modulated lightwave AM-VSB CATV systems," *IEEE Photon. Technol. Lett.*, vol. 8, pp. 697–699, May 1996.

[9] G. C. Wilson, "Optimized predistortion of overmodulated Mach-Zehnder modulators with multicarrier input," *IEEE Photon. Technol. Lett.*, vol. 9, pp. 1535–1537, Nov. 1997.

[10] A. A. M. Saleh, "Fundamental limit on number of channels in subcarrier-multiplexed lightwave CATV system," *Electron. Lett.*, vol. 25, pp. 776–777, June 1989.

[11] N. J. Frigo, M. R. Phillips, and G. E. Bodeep, "Clipping distortion in lightwave CATV systems: Models, simulations, and measurements," *J. Lightwave Technol.*, vol. 11, pp. 138–146, Jan. 1993.

[12] A. J. Rainal, "Distortion spectrum of laser intensity modulation," *IEEE Trans. Commun.*, vol. 43, no. 2/3/4, pp. 1644–1652, Feb. 1995.

[13] K. P. Ho and J. M. Kahn, "On models of clipping distortion for lightwave CATV systems," *IEEE Photon. Technol. Lett.*, vol. 8, pp. 125–126, Jan. 1996.

[14] M. Maeda and M. Yamamotto, "FM-FDM optical CATV transmission experiment and system design for MUSE HDTV signals," *IEEE J. Select. Areas Commun.*, vol. 8, pp. 1257–1267, Sept. 1990.

[15] S. L. Woodward, V. Swaminathan, G. E. Bodeep, and A. K. Singh, "Transmission of QPSK signals using unisolated DFB lasers," *IEEE Photon. Technol. Lett.*, vol. 8, pp. 127–129, Jan. 1996.

[16] S. L. Woodward, X. Lu, T. E. Darcie, and G. E. Bodeep, "Reduction of optical-beat interference in subcarrier networks," *IEEE Photon. Technol. Lett.*, vol. 8, pp. 694–696, May 1996.

[17] C. C. Hsiao, B. H. Wang, and W. I. Way, "Multiple access in the presence of optical-beat and co-channel interference using Walsh-code-based synchronized CDMA technique," *IEEE Photon. Technol. Lett.*, vol. 9, pp. 1173–1175, Aug. 1997.

[18] B. H. Wang, C. C. Hsiao, and W. I. Way, "Suppression of optical beat interference using synchronized CDMA technique and in-band clipping carrier," *Electron. Lett.*, vol. 33, no. 32, pp. 1888–1890, Oct. 1997.

[19] T. H. Wood and N. K. Shankaranarayanan, " Operation of a passive optical network with subcarrier multiplexing in the presence of optical beat interference," *J. Lightwave Technol.*, vol. 11, pp. 1632–1640, Oct. 1993.

[20] M. K. Haldar, K. B. Chia, and F. V. C. Mendis, "Dynamic considerations in overmodulation of semiconductor laser diodes," *Electron. Lett.*, vol. 32, no. 7, pp. 659–661, Mar. 1996.

[21] T. Anderson and D. Crosby, "The frequency dependence of clipping induced bit-error rates in subcarrier multiplexed systems," *IEEE Photon. Technol. Lett.*, vol. 8, pp. 1076–1078, Aug. 1996.

[22] S. Betti, E. Bravi, and M. Giaconi, "Effect of the turn-on delay of a semiconductor laser on clipping impulsive noise," *IEEE Photon. Technol. Lett.*, vol. 9, pp. 103–105, Jan. 1997.

[23] J. Le Bihan, "Approximate dynamic model for evaluating distortion in a semiconductor laser under overmodulation," *IEEE Photon. Technol. Lett.*, vol. 9, pp. 303–305, Mar. 1997.

[24] B. Pucel, "Comparison between static and dynamic clipping distortion in semiconductor lasers," *IEEE Photon. Technol. Lett.*, vol. 9, pp. 1532–1534, Nov. 1997.

[25] O. Shimbo, *Transmission Analysis in Communication Systems*. Rockville, MD: Computer Science, 1988.

[26] J. Wang, M. K. Haldar, and F. V. C. Mendis, "Formula for two-carrier third-order intermodulation distortion in semiconductor laser diodes," *Electron. Lett.*, vol. 29, no. 15, pp. 1341–1343, 1993.

Benjamin H. Wang (S'95–M'97) was born in Taiwan, China, in 1968. He received the B.S. and M.S.E.E. degrees in electrical engineering from Tatung Institute of Technology, Taiwan, in 1990 and 1992, respectively, and the Ph.D. degree in electronics engineering from National Chiao-Tung University, Taiwan, in 1998.

His current interest is in the area of subcarrier-multiplexed-based optical access networks and gigabit DWDM networking systems. He is now with Computer and Communication Research Laboratories at Industrial Technology Research Institute, Taiwan.

Pi-Yang Chiang (S'95–M'98) was born in Taiwan, China, in 1968. He received the B.S. degree in electrical engineering from National Taiwan University, Taiwan, in 1990, and the M.S.E.E. and Ph.D. degrees in communication engineering from National Chiao-Tung University, Taiwan, in 1992 and 1998, respectively.

He is currently interested in the area of hybrid fiber coax networks and subcarrier optical communication systems. He is now with Askey Computer Corporation, Taiwan.

Ming-Seng Kao (S'89–M'90) was born in Taipei, Taiwan, China, in 1959. He received the B.S.E.E degree from National Taiwan University, China, in 1982, the M.S. degree in optoelectronics from National Chiao-Tung University, in 1986, and the Ph.D. degree in electrical engineering from National Taiwan University, in 1990.

From 1986 to 1987, he was an Assistant Researcher at the Telecommunications Laboratories, Chung-Li, Taiwan. In 1990, he joined the Faculty of National Chiao-Tung University, Hsinchu, Taiwan, where he is now a Professor of Communication Engineering Department. Between 1993–1994, he was a Visiting Professor at the Swiss Federal Institute of Technology (ETH), Zurich, Switzerland, where he worked in the area of optical communications. He is currently interested in high-speed optical networks.

Winston I. Way (S'82–M'83–SM'88) received the B.S. degree from National Chiao-Tung University, Taiwan, in 1977, and the M.S.E.E. and Ph.D. degrees in electrical engineering and science from the University of Pennsylvania, Philadelphia, PA, in 1981 and 1983, respectively.

From 1984 to 1992, he was with Applied Research Division at Bellcore, where he was involved in various lightwave system research projects such as pioneering in distributing satellite, digital radio, and cable television signals by using subcarrier multiplexing techniques; designing hybrid/IC regenerators for direct detection systems; designing lightwave systems that include erbium-doped fiber amplifiers, semiconductor optical amplifiers; studying system and network issues related to dense wavelength division multiplexing and optical frequency division multiplexing techniques; and studying the feasibility of applying advanced lightwave technologies to SONET/SDH self-healing rings. Since 1992, he has been with the Department of Communications Engineering, the National Chiao-Tung University, Hsinchu, Taiwan, China, where he is a Professor and has been leading a number of projects on HFC access system technologies and high-speed WDM networking. He is the author of the book *Broadband HFC Access System Technologies*. He has also published a book chapter and over 90 refereed technical papers in international journals and conferences and has held three United States patents.

Dr. Way has been serving as Chair or Technical Program Committee Member in numerous IEEE/LEOS and IEEE/MTT international conferences and was an IEEE Guest Editor. He is a Fellow of the Optical Society of America (OSA).